Bioelectrochemistry 135 (2020) 107547

Contents lists available at ScienceDirect

Bioelectrochemistry

journal homepage: www.elsevier.com/locate/bioelechem

Mass transport of lipopolysaccharide induced H_2O_2 detected by an intracellular carbon nanoelectrode sensor

J.M. Hicks [a], N.J. Silman [b], S.K. Jackson [c], J.W. Aylott [a], F.J. Rawson [a,*]

[a] School of Pharmacy, Biodiscovery Institute, University of Nottingham, NG7 2RD, UK
[b] Public Health England, Porton Down, Salisbury SP4 0JG, UK
[c] Medicine and Dentistry, Portland Square, Drakes Circus, University of Plymouth, PL4 8AA, UK

ARTICLE INFO

Article history:
Received 29 January 2020
Received in revised form 30 April 2020
Accepted 30 April 2020
Available online 4 May 2020

Keywords:
LPS
Biosensor
Hydrogen peroxide
Carbon nanotubes
Diffusion

ABSTRACT

Hydrogen peroxide is a key component of the innate immune response, regulating how a cell responds to a bacterial threat; however, being transient in nature makes it extremely difficult to detect. We show the development of an improved biosensor capable of the rapid detection of the hydrogen peroxide produced intracellularly in response to both smooth and rough lipopolysaccharides (LPS) structures. The arising signal and mass transport behaviour to the electrodes were characterised. This response was detected utilising a single walled carbon nanotube-based sensor that has been functionalised with an osmium complex for specificity and detecting the change in intracellular concentrations of hydrogen peroxide through chronoamperometry. This was conducted within murine macrophage (RAW264.7) cells and using ultra-pure LPS extracted from two different serotypes of bacteria (0111:B4 and Re495). This allowed the comparison of the immune response when infected with different structures of LPS. We demonstrate that the hydrogen peroxide signal can be electrochemically detected within 3 seconds post injection. Combining the nature of the mass transport of hydrogen peroxide and concentration characteristics, a bacterial 'fingerprint' was identified. The impact of this work will be demonstrated in allowing us to develop a rapid diagnostic for bacterial detection.

1. Introduction

Direct measurement, in real-time, of intracellular analytes has always been a challenge. Endpoint measurements, where analytes are measured after a set time and normally involve the destruction of the cellular system, have been widely popular due to their accuracy and ease of implementation [1]. However, these have the major disadvantage of not being able to measure the dynamic processes within cells in real-time. This can be overcome through the use of bio-electrochemical techniques which have evolved over the last few decades with the development of biosensors capable of measuring analytes without the destruction of the cell [2]. Such sensors have had success in measuring extracellular analytes [3,4] while intracellular analytes have remained a challenge. There are three key obstacles in developing an effective intracellular biosensor: 1- sensors need to be extremely small to be internalised within cells (nm scale); 2- be able to distinguish the analyte of interest within a complex system such as the cytosol and 3- have low limits of detection relative to intracellular concentrations (pM-nM).

Reactive oxygen species (ROS) are a key target analyte for intracellular biosensors as they play a major role in numerous cellular processes [5] including cell signaling [6], inflammation [7] and the immune response [8,9]. Lipopolysaccharides (LPS) from the outer membrane of Gram-negative bacteria are a key initiator of the innate immune response triggering intracellular production of ROS including hydrogen peroxide [10], through their interaction with the transmembrane protein receptor Toll-Like Receptor 4 (TL4). It is hypothesised that the different structures of LPS trigger different intracellular ROS responses. Broadly LPS structures are characterised into wild type/smooth and rough which are structurally truncated forms of the wild type forms [11]. While broadly categorised as 'smooth' or 'rough' LPS there is a huge variety in structures that are present in bacteria allowing for a broad range of intracellular responses.

A common technique for the detection of biological agents is the use of fluorescent probes. There are many different probes readily available for use in research (a comprehensive table of probes is seen in SI Fig. S1). Being able to visualise fluorescence on a microscope is a valuable advantage in determining the loca-

* Corresponding author.
E-mail address: Frankie.rawson@nottingham.ac.uk (F.J. Rawson).

https://doi.org/10.1016/j.bioelechem.2020.107547
1567-5394/

tion of an analyte and its distribution. Fluorophores are also easily attached to particles or other delivery mechanisms making them easily adaptable to the requirements of the research [12,13]. However, the specificity of fluorescent probes for ROS detection leaves much to be desired with many probes reacting with multiple different ROS.

Fluorescent sensors, while very useful, fail in their ability to distinguish between ROS in complex solutions. Electrochemical biosensors seem to hold greater potential in fulfilling this niche due to their adaptability and ability to sense specific analytes in a time-sensitive manner.

There are many types of electrochemical sensor [14] that can be used in the detection of bacteria. A few examples would be a sensor that electrochemically sequences the bacteria's RNA [15], a sensor with bioreceptors targeted to the bacteria [16] or molecular imprinted polymers [17]. Electrochemical biosensors compose of a signal processor, a transducer element and a recognition element and are a common choice for the detection of bacteria. The recognition element gives specificity towards the analyte of interest and can be adapted as required. For the detection of Gram-negative bacteria this recognition element can be targeted either to the whole bacteria itself, the LPS structures, or to the ROS response (including hydrogen peroxide) that is produced by the host immune system after infection.

There has been a great deal of research developing electrodes specific for LPS detection with varying success. A commercial kit for LPS detection is available based on a colorimetric assay. This is based on the protein limulus amebocyte lysate (LAL) which reacts with the endotoxins from bacteria [18]. This LAL assay, however, cannot differentiate between bacterial serotypes [19]. Other tests for LPS detection utilise a variety of techniques to achieve specificity including aptamers and bacteriophages (see SI Fig. S2).

Aptamers are single stranded oligonucleotides that are designed to bind to a specific molecule with high specificity and affinity [20]. They have been designed as an alternative to using antibodies which are extremely expensive to develop and are up to one hundred times smaller than antibodies. Aptamers have proven to be an efficient recognition element [21] and are re-useable [22]. However, to date, only one aptamer has been approved for therapeutic use [23] with the main disadvantage being the extreme difficulty in their synthesis [20]. Bacteriophages have proven to be a successful alternative to both LAL and aptamer-based assays being extremely sensitive and easily modified as an addition to an electrode surface [24]. There is limited sensitivity between serotypes and often involves the lysis of bacterial and host cells which could induce an immune inflammatory response if used in a clinical setting [25]. Current LPS testing is sensitive to less than 1 ng/ml of LPS in suspension however, the key issue is distinguishing between serotypes.

Testing for the immune ROS response to bacteria rather than the LPS itself is a more dynamic method and holds greater promise as a clinical diagnostic test. We have identified a ROS burst produced in response to bacterial infection within seconds [26,27] of infection. The timeframe and specific ROS produced is thought to be indicative of the infection, acting almost like a 'fingerprint' in identifying the bacteria involved. A summary of the current electrochemical techniques for hydrogen peroxide detection is shown in SI Fig. S3.

Previously, our group has shown that a carbon nanotube-based biosensor can detect an intracellular hydrogen peroxide burst produced on a short time scale [27] in a concentration dependent manner. These sensors are based on vertically aligned, immobilised single walled carbon nanotubes (CNTs) on an indium tin oxide (ITO) substrate and further modified with a pyridine complex with a redox active osmium core, for specificity towards hydrogen peroxide (H_2O_2). The CNTs are attached to the ITO through a poly-arylamine (pAA) tether layer that is electrochemically grafted to the ITO surface. These CNTs can be physically inserted into mammalian cells (RAW264.7) where they are then capable of detecting intracellular analytes [27]. We have also shown that the traditional method of grafting the pAA layer to the surface passivates the electrode kinetics. We demonstrated that through the manipulation of the pAA the kinetics of the biosensor could be improved and a detection limit of 368 nm for hydrogen peroxide was achieved [26,28]. Here we describe that the improved electron transfer kinetics of the biosensor allow for a faster detection response (3 s), direct measurement of the mass transport characteristics of the hydrogen peroxide to the biosensor and the characterisation of the response differences between smooth and rough LPS.

Combined, this will allow the further development of an accurate and precise bacterial sensor. Beyond bacterial sensing, this biosensor has the potential to be modified to detect numerous different ROS (by changing the functional group) and to be used in any number of applications where detecting intracellular ROS is important.

2. Materials and methods

2.1. Materials

Unless otherwise stated all materials were obtained from Sigma-Aldrich.

2.2. Cell culture

Raw 264.7 cells (EACC) were cultured in T75 flasks (Corning) in 20 ml of high glucose DMEM media (containing 10% FBS, 2.5% HEPES) in a cell culture incubator at 37 °C and 5% CO_2. Cells were allowed to grow for 2–3 days until reaching 80% confluency and were harvested with a cell scraper (Corning). Cells were counted using a haemocytometer with 10 μL of cells mixed with 10 μL of trypan blue to measure the number of viable cells per ml.

2.3. Sensor construction

Preparation of the nanotubes and constructing the biosensor has been described in detail previously [28]. Briefly, SWCNTs (Nanolab Inc.) were chemically cut in a concentrated acid mix (nitric and sulphuric acid, 1:3 ratio) by sonication for 10 h. These were then attached to an indium tin oxide (ITO, Delta Technologies Ltd) surface via an in-situ generated, diazonium tether layer that forms a poly-arylamine (pAA) multi-layer upon application of −0.6 V for a fixed time. This layer can either be a thick layer (approximately 21 nm) or a thin layer (approximately 3 nm) [28]. Synthesis of Osmium(II)bis-2,2-bipyridine(p-aminomethyl pyridine)chlorido hexafluorophosphate (Os) was conducted and coupled to the SWCNTs as described previously [29]. The final sensor construct is abbreviated as ITO-SWCNT-Os.

2.4. Electrochemical studies

Electrochemical experiments were conducted using a Metrohm Autolab M204 potentiostat running Nova 2.1 software. A three-electrode system was used in all cases with the working electrode being the ITO-SWCNT-Os sensor, the reference electrode was a Ag/AgCl and a platinum wire was used as a counter electrode. Cyclic voltammetry (Fig. 2A/B) was conducted between 0.6 V and 0.0 V scanning in the negative direction at 0.1 V s^{-1}. A 1 ml solution of PBS was used as a supporting electrolyte. The chronoamperograms in Fig. 2 C was also conducted with 1 ml PBS as the supporting electrolyte. A fixed potential of either 0.15 V or 0.4 V was applied and

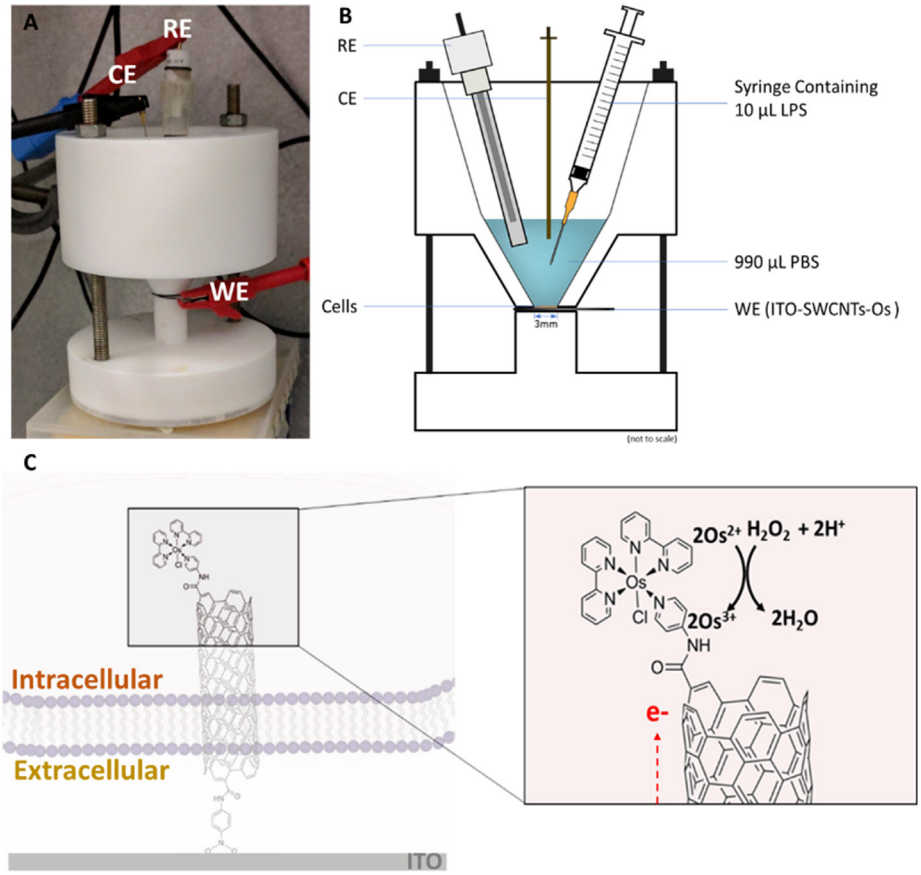

Fig. 1. Practical set up of electrochemical cells; WE = working electrode, RE = reference electrode and CE = counter electrode. (A) Photo of electrochemical set up within the Faraday cage. (B) Labelled cartoon schematic of the set-up. (C) Schematic demonstrating the ITO-SWCNT-Os biosensor as it crosses the plasma membrane. Osmium core of the osmium complex is the site of hydrogen peroxide reaction.

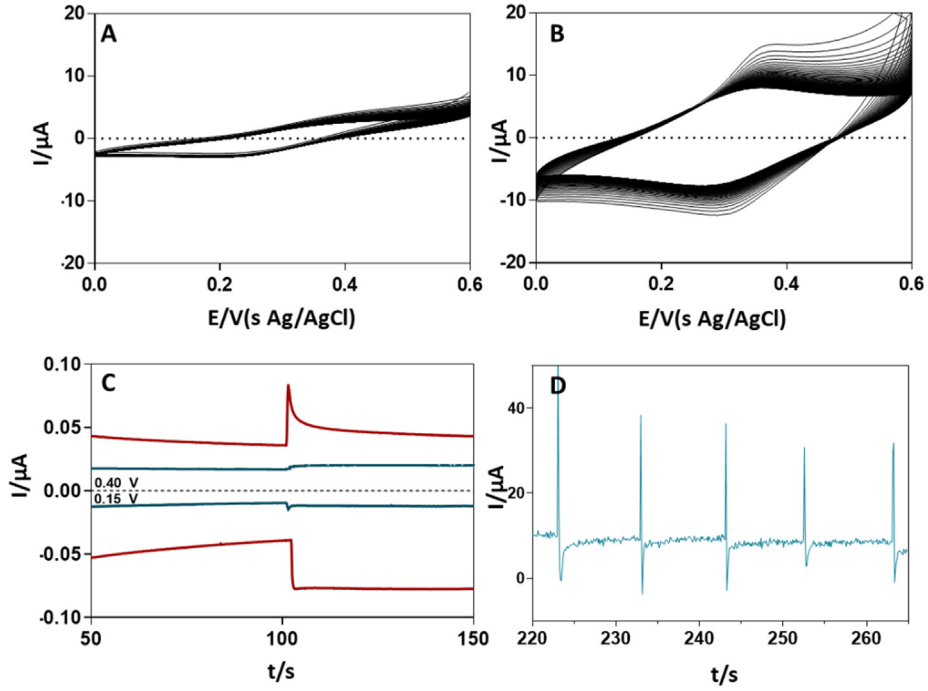

Fig. 2. Detection differences between sensors made with a thick or thin arylamine tether layer. A & B 100 consecutive CVs of ITO-SWCNT-Os sensor in PBS between 0 V and 0.6 V at 0.1 V/s-1. (A) Sensor constructed with a thick arylamine tether layer; (B) constructed with a thin arylamine tether layer. (C) Chronoamperograms with voltage held at either 0.4 V (top half) or 0.15 V (bottom half). Red lines represent 3 nm-pAA-CNT-Os sensor and blue lines represent 21 nm-pAA-CNT-Os sensor. (D) Typical chronoamperogram at 0.15 V in a PBS electrolyte. Working electrode of ITO-CNT-Os sensor with a thin pAA layer. Interval time of 0.1 s. Repetitive stimulations with 100 µM hydrogen peroxide. Study repeated three times. Stimulations shown are the final 5 stimulations after more than 30 stimulations.

100 μL aliquots of 100 μM hydrogen peroxide were pipetted in. Similarly, Fig. 2D was conducted with 5 ml PBS and 100 μL aliquots of 100 μM hydrogen peroxide were pipetted in.

Baseline correction was conducted on chronoamperograms (Figs. 3A and 4A) using the Nova2.1 software. This uses the measured data points before stimulation to plot a baseline (linear mode) and adjusts the data set by subtracting the calculated baseline.

2.5. Hydrogen peroxide detection

ITO-SWCNT-Os sensors (ITO base measuring approximately 1 cm × 1.5 cm) were placed within a 6-well plate (Corning). 1×10^6 cells in 2 ml of media was then pipetted on top to cover the sensor completely. Insertion of the SWCNTs within the cells was achieved by centrifugation of the sensors/cells at 1000 rpm for 3 min (Sorvail Legend RT). Excess cells not inserted are then washed away by gentle agitation in PBS. Sensors were stored for up to an hour in PBS until use. When ready to use sensors were assembled submerged in 990 μL of PBS as shown in Fig. 1. A fixed potential of 0.15 V was applied for up to 20 min prior to injection of 10 μL of ultra-pure LPS; smooth (*E. coli* 0111:B4) or rough (*S. minnesota* Re595; Quadratech Diagnostics, final concentration of 1 μg/ml). This was done to ensure an accurate baseline current was recorded. Current was continuously measured for 5 min post-injection. A schematic showing the practical set up is shown in Fig. 1.

2.6. Analysis

Further analysis was conducted with Graphpad prism (v7) software. To simplify the analysis of the mass transport response we have assumed linearity in diffusion response in the region of the graph where there is greatest change (Figs. 3C and 4C).

3. Results and discussion

Previously, our group has shown it is possible to detect the hydrogen peroxide burst produced within mammalian cells in response to bacterial lipopolysaccharides (LPS). This was achieved through a biosensor constructed of immobilised single walled carbon nanotubes (SWCNTs) that were modified with an osmium complex (see Fig. 1C). However, the mass transport characteristics of the intracellular hydrogen peroxide produced have never been investigated.

The poly-arylamine (pAA) layer used to tether the SWCNTs to the ITO is generated by the in-situ formation of diazonium which is then grafted to the ITO surface by applying a fixed potential. The longer a potential is applied, the thicker the resulting pAA layer [28]. By limiting the thickness of the pAA tether layer we show the enhancement of the detection capabilities for an improved bacterial biosensor that we have previously developed [27]. The original biosensor constructed with a tether layer approximately 21 nm thick is referred to as 'thick' and the new biosensor with a tether layer approximately 3 nm is referred to as 'thin'.

A cross-section schematic of the practical set-up of the electrochemical cell can be seen in Fig. 1. Here the biosensor is immobilised with a fixed surface area of 7 mm^2 exposed to the electrolyte.

3.1. Improvement of biosensor

All sensors were primed before use by running 100 consecutive cyclic voltammograms (CV) in sterile phosphate buffered saline (PBS) (Fig. 2A and B) [27]. These CV's show the oxidation and reduction of the osmium core of the ITO-SWCNT-Os sensor (see Fig. 2A and B). From Fig. 2A and B, the electrode surface is saturated at approximately 0.3 V for both oxidation and reduction. By applying a fixed potential of 0.15 V it ensures the osmium core of the electrode maintains its reduced state and by applying a fixed potential

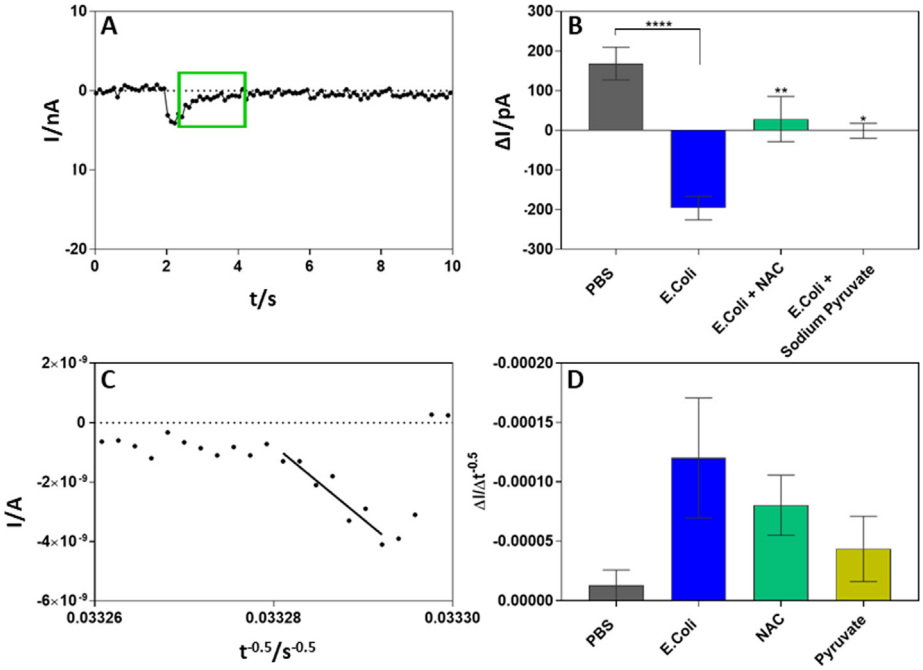

Fig. 3. Macrophage response to smooth LPS from *E. coli*. (A) Typical chronoamperogram after baseline correction (see Section 2). (B) Bar graph displaying the mean change in current after injection of either the PBS control (n = 7) or smooth LPS (n = 7). NAC (n = 9) and sodium pyruvate (n = 6) bars indicate samples where cells have been pre-incubated prior to injection with the labelled substance. (C) Typical Cottrell plot after LPS injection including time period indicated by green box in A. (D) Bar graph of diffusion slopes measured in C. Bar graphs display mean ± SEM. Significance tested with a one-way ANOVA and Tukey post-test. P < 0.03 = *, p < 0.002 = **, p < 0.0002 = ***, p < 0.0001 = ****.

of 0.4 V it ensures the osmium core is maintained in its oxidative state. We have reported the electrochemical mechanism of hydrogen peroxide detection previously [27]. Briefly, the osmium core acts as a catalase mimic causing hydrogen peroxide disproportionation. The redox state of the osmium core is dependent on the potential applied leaving it ready to be readily oxidised (and re-reduced at 0.15 V) or readily reduced (and re-oxidised at 0.4 V) by the hydrogen peroxide. Both the peak reduction and peak oxidation of the osmium complex (where there is maximum current at the electrode surface) are much greater from the sensors constructed with a thin aryl layer having a peak oxidation current 1.55 μA larger than the thick aryl layer sensors. Taking measurements from the 100th CV it was found that the peak oxidation current for the thick aryl layer sensor was 0.51 μA (SD = 0.2 μA) while the sensor with the thin aryl layer had a peak oxidative current of 2.06 μA (SD = 0.6 μA). The peak separation was also smaller from 120 mV (SD = 40. mV) to 103 mV (SD = 17 mV) indicating an increase in electrochemical reversibility. Fig. 2C displays fixed potential chronoamperograms obtained using ITO-SWCNT-Os working electrodes made with either the thin (3 nm) pAA or the thick (21 nm) pAA exposed to an electrolyte solution of PBS (1 ml). While the chronoamperogram was running hydrogen peroxide aliquots were introduced to the solution by pipetting (100 μL of 100 μM); this can be seen by the spikes in current shown in Fig. 2C. The thin aryl layer displayed a greater current response when the sensor was being held at 0.4 V (oxidation, 44.3 nA increase) and 0.15 V (reduction, 34.6nA increase). This is further reflected in the improved limit of detection to 368 nm [26] from 25 μm [26]. Fig. 2D shows a fixed potential chronoamperometry at 0.15 V using an ITO-SWCNT-Os sensor made with a thin pAA. Hydrogen peroxide was repetitively pipetted into the solution (5 ml PBS) while the chronoamperogram was recording. This demonstrates the reusability of the sensor as it can detect repetitive stimulations of hydrogen peroxide. We then wished to explore how the sensors with the thinner layer of pAA behaved intracellularly.

3.2. Smooth LPS hydrogen peroxide response

We hypothesised that we could measure differences in hydrogen peroxide response between different LPS serotypes, whether this was a change in hydrogen peroxide concentration or timescale of response. To compare two serotypes of LPS we chose to investigate LPS obtained from *E. coli* 0111:B4 (smooth) and *S. minnesota* Re595 (rough). These serotypes were chosen as they were readily available and thoroughly researched in the literature. The sensors were internalised within the cells by centrifugation, as described previously, with the successful internalisation measured by methylene blue analysis (see SI Fig. S4) which our group and others have previously validated this method [27,30,31]. This involves cells up taking the redox active molecule, methylene blue, with excess washed away. If the CNTs have successfully penetrated the cell membrane they will be able to stimulate the reduction of methylene blue to leucomethylene blue. The characteristic reduction peak of methylene blue is observed with sensors made with either a thin pAA layer or a thick pAA layer indicating the CNTs have been successfully internalised. The improved biosensor with the thin-pAA layer was used and mass transport behaviour of H_2O_2 induced production on LPS stimulation of macrophage investigated. For a diffusion controlled processes that displays linear diffusion, the Cottrell equation [32] applies (see Eq. (1)) where the current measured is directly proportional to concentration. This equation also directly links diffusion to both current and time making it possible the investigate the nature of the mass transport to our electrodes.

Eq. (1) Cottrell equation. n = number of electrons, F = Faraday constant, A = area of electrode (cm^2), C = concentration of analyte (mol/cm^3), D = diffusion coefficient (cm^2/s), t = time (s).

$$i = \frac{nFAC\sqrt{D}}{\sqrt{\pi t}} \quad (1)$$

By measuring the current response after LPS injection by chronoamperometry we were able to measure the mass transport characteristics of hydrogen peroxide to the CNT modified electrode by analysing the current observed with time after injection of LPS (see Fig. 3). Each repeat was conducted with a sensor made on a different day to consider variability between batches. From the chronoamperometric data, we could quantify the response time, characterise the response diffusion characteristics and response current. Together forming a response 'fingerprint' for bacterial detection. The mass transport of the hydrogen peroxide to the osmium core of the biosensor is dominated by diffusion. This diffusion can be observed when you plot current vs time$^{0.5}$, regions of the resulting graph where an inverse proportional relationship is seen are indicative of the mass transport (see Eq. (1)). From this we can then measure two components, one: was the time of which diffusion is measurable and two: the slope of the diffusion ($\Delta I/\Delta t^{-0.5}$) as an indicator of the flux of hydrogen peroxide to the biosensor.

The time of injection is labelled as 0 s and in all cases, a response is seen within 3 s (defined as the time when a significant deviation of current from the baseline is observed). Mass transport effects (dominated by diffusion) are observable between 2 and 4 s and are highlighted by a green box in Fig. 3A and the detection of mass transport is shown in Fig. 3C. Various controls were implemented to prove the signal measured was a result of an increase in localised intracellular hydrogen peroxide. Phosphate buffered saline (PBS) was used as a blank control; N-acetylcysteine (NAC) was used as a general antioxidant and should negate a response from any ROS while sodium pyruvate is a membrane diffusible scavenger of hydrogen peroxide.

From Fig. 3 it can be seen that a controlled dose of smooth LPS (1 μg/ml) from *E. coli* results in observed diffusion of hydrogen peroxide lasting approximately 2 s (see Fig. 3A and C) and a negative change in average current that is significantly different from the PBS control (Δ364 pA, $p < 0.0001$). Both the NAC and sodium pyruvate controls gave very little change in current after smooth LPS injection and are significantly different from the smooth LPS samples; (NAC + 28 pA, $p < 0.002$; sodium pyruvate − 1.2 pA, $p < 0.03$). While there are clear differences in the current response with the different sample groups, there is no significant difference in diffusion response. While it seems from Fig. 3D that the smooth LPS gives a much steeper diffusion slope, $\Delta I/\Delta t^{-0.5}$, than the control groups, the variation is shown in the standard error of the mean (SEM) shows that this diffusion response is extremely variable and that there is still some diffusion occurring and being detected by the biosensor even in the control groups.

3.3. Rough LPS hydrogen peroxide response

Immediate response differences from rough LPS can be seen in the typical chronoamperogram as shown in Fig. 4A which shows a diminished change in current after injection of LPS. The length of time where diffusion is detected (indicated by the green box) is much shorter (~1 s). Despite this shorter time where diffusion is seen, a steeper diffusion slope from the Cottrell plot is observed (Fig. 4C). This indicates a steeper concentration gradient and therefore a faster change in concentration of hydrogen peroxide at the sensor surface. The minimal amount of diffusion of hydrogen peroxide seen in the controls shows (Fig. 4D) that the majority, if not all of what we are measuring in our test conditions is from hydrogen peroxide.

Given the research in the literature comparing macrophage behaviour in response to smooth and rough LPS, it was expected that the rough LPS would give a larger current response corre-

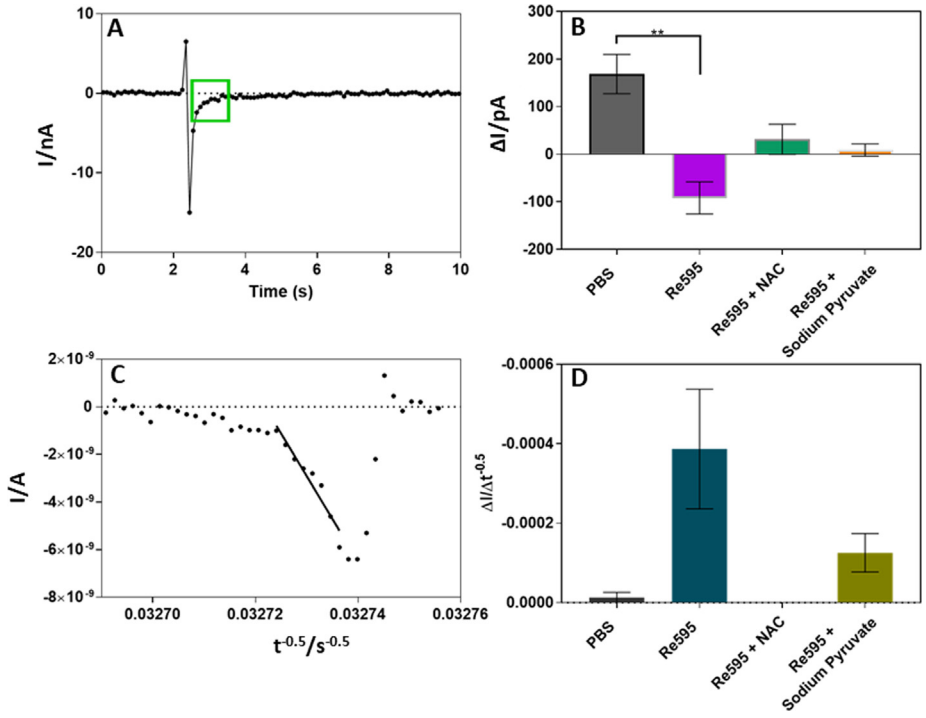

Fig. 4. Macrophage response to rough LPS from *S. minnesota* Re595. (A) Typical chronoamperogram after baseline correction. (B) Bar graph displaying the mean change in current after injection of either the PBS control (n = 7) or rough LPS (n = 9). NAC (n = 5) and sodium pyruvate (n = 5) bars indicate samples where cells have been pre-incubated prior to injection with the labelled substance. (C) Typical Cottrell plot after LPS injection including time period indicated by green box in A. (D) Bar graph of diffusion slopes measured in C. Bar graphs display mean ± SEM. Significance tested with a one-way ANOVA and Tukey post-test. P < 0.03 = *, p < 0.002 = **, p < 0.0002 = ***, p < 0.0001 = ****

Table 1
Summary table of change in current and observable diffusion values from Cottrell slopes after either smooth (*E. coli*) or rough (*S. minnesota*) LPS injection. Numbers represent mean (n ≥ 6), values in brackets represent SEM).

	Smooth LPS	+NAC	+Sodium Pyruvate	*Rough LPS*	+NAC	+Sodium Pyruvate
Change in Current (pA)	−196.0 *(±29.62)*	+28.0 *(±56.9)*	−1.2 *(18.94)*	−91.0 *(±33.76)*	+31.0 *(±31.6)*	+8.9 *(±30.5)*
Diffusion ($A/s^{0.5}$)	-1.2×10^{-4} *(5.0×10^{-5})*	-8.0×10^{-5} *(2.5×10^{-5})*	-4.4×10^{-5} *(2.7×10^{-5})*	-3.9×10^{-4} *(1.5×10^{-4})*	0	-1.3×10^{-4} *(4.8×10^{-5})*

sponding to a larger production of hydrogen peroxide [33,34]. This is generally thought to be a result of the fact that rough LPS can bypass the normal cell machinery in escorting and controlling LPS delivery to immune cells (see review [35]). The change in current from the rough LPS was −91 pA; a significant difference of 259 pA versus the PBS control ($p < 0.002$) but 104 pA more positive than the smooth LPS response. This difference in current response gives us an indication of hydrogen peroxide production in response to bacterial threat and the differences in response between smooth LPS and rough LPS. There is an interesting contrast between the rate of diffusion and the intensity of response for both the smooth and rough LPS. The smooth LPS appears to have a slower diffusion of hydrogen peroxide than the rough but a much larger current response (see Table 1). This is contradictory to what is historically thought about LPS response that rough LPS has previously been thought to give a much larger ROS response than smooth. However, this has always been when studying much longer timescales as until recently [26,27] ROS and hydrogen peroxide responses were not able to be studied on such short timescales of within seconds of infection. In all cases the change in current with LPS is statistically significant versus the PBS control and with the change in current in the NAC and sodium pyruvate controls being minimal.

When comparing these results to the current technologies in the literature for intracellular hydrogen peroxide sensors the ability of this sensor to detect the diffusion of hydrogen peroxide is a novel and significant development. Traditional fluorophore based methods have a variety of detection limits (see SI Fig. S1), times and specificity but they have been shown to be able to detect as little as 5 pmol of hydrogen peroxide within 2 min [36]; though the majority of fluorophores have a minimum detection time of 3-5 min [37]. Due to this, the detection of the diffusion of hydrogen peroxide is just not possible with this technique at current. Current electrochemical techniques that are capable of intracellular measurements of hydrogen peroxide (see SI Fig. S3), at current do not have nanomolar level of detection limits, with the majority being in the micromolar range [38,39]. There is also no current literature displaying the detection of the diffusion of intracellular hydrogen peroxide to the electrode surface. Amatore's group have developed an intracellular ROS nanoelectrode capable of detecting a range of ROS, including hydrogen peroxide, though mass transport and the limit of detection were not investigated [40]. Recently, a group in Iran have developed a sensor capable of nanomolar detection of hydrogen peroxide but did not report on the mass transport properties [40,41]. This highlights the significance of this work and the ability to investigate the mass transport characteristics of hydrogen peroxide produced intracellularly in response to a bacterial threat.

4. Conclusion

Here we have shown that by limiting the pAA layer the resulting enhanced electron transfer kinetics [28] allow for the detection

of the diffusion of hydrogen peroxide produced by bacterial LPS. This sensor has also improved the response time to stimulus to under 3 s. The rough and smooth LPS result in different combinations of diffusion and current response profiles with the smooth LPS giving a high current response with slow diffusion while the inverse is true for the rough LPS (see Table 1). This suggests the flux of hydrogen peroxide to the electrode is different with each serotype and possibly suggesting that the hydrogen peroxide is produced in numerous locations for the higher concentration to present a lower flux. While merely detecting the hydrogen peroxide response to bacterial LPS may provide an 'incomplete' fingerprint it is an important step in real-time intracellular sensing and is an extremely adaptable biosensor. Future work on this should include expanding the fingerprint to multiple ROS molecules including superoxide in order to have a detailed response profile for different bacterial LPS structures and investigating the different methods of hydrogen peroxide production in response to a bacterial threat.

Declaration of Competing Interest

The authors declare that they have no known competing financial interests or personal relationships that could have appeared to influence the work reported in this paper.

Acknowledgements

This work was supported by the Engineering and Physical Research grant number EP/R004072/1 and Biotechnology and Biological Sciences Research Council grant number BB/L017059/1

Appendix A. Supplementary material

Supplementary data to this article can be found online at https://doi.org/10.1016/j.bioelechem.2020.107547.

References

[1] K.K. Griendling, R.M. Touyz, J.L. Zweier, S. Dikalov, W. Chilian, Y.R. Chen, D.G. Harrison, A. Bhatnagar, Measurement of reactive oxygen species, reactive nitrogen species, and redox-dependent signaling in the cardiovascular system: a scientific statement from the American Heart Association, Circ. Res. 119 (5) (2016) e39–e75.
[2] N.J. Ronkainen, H.B. Halsall, W.R. Heineman, Electrochemical biosensors, Chem. Soc. Rev. 39 (5) (2010) 1747–1763.
[3] C. Li, H. Zhang, P. Wu, Z. Gong, G. Xu, C. Cai, Electrochemical detection of extracellular hydrogen peroxide released from RAW 264.7 murine macrophage cells based on horseradish peroxidase-hydroxyapatite nanohybrids, Analyst 136 (6) (2011) 1116–1123.
[4] C. Amatore, S. Arbault, Y. Chen, C. Crozatier, I. Tapsoba, Electrochemical detection in a microfluidic device of oxidative stress generated by macrophage cells, Lab Chip 7 (2) (2007) 233–238.
[5] K. Brieger, S. Schiavone, F.J. Miller Jr., K.H. Krause, Reactive oxygen species: from health to disease, Swiss Med. Wkly 142 (2012) w13659.
[6] M. Schieber, N.S. Chandel, ROS function in redox signaling and oxidative stress, Curr. Biol. 24 (10) (2014) R453–R462.
[7] P.D. Ray, B.W. Huang, Y. Tsuji, Reactive oxygen species (ROS) homeostasis and redox regulation in cellular signaling, Cell. Signal. 24 (5) (2012) 981–990.
[8] D.G. Franchina, C. Dostert, D. Brenner, Reactive oxygen species: involvement in T cell signaling and metabolism, Trends Immunol. 39 (6) (2018) 489–502.
[9] Y. Chen, Z. Zhou, W. Min, Mitochondria, oxidative stress and innate immunity, Front. Physiol. 9 (2018).
[10] D. Heumann, T. Roger, Initial responses to endotoxins and Gram-negative bacteria, Clin. Chim. Acta 323 (1–2) (2002) 59–72.
[11] A.P. Moran, Molecular structure, biosynthesis, and pathogenic roles of lipopolysaccharides, in: Helicobacter pylori, ASM Press, 2001.
[12] Y.-E.K. Lee, R. Kopelman, R. Smith, Nanoparticle PEBBLE sensors in live cells and in vivo, Annu. Rev. Anal. Chem. 1 (2) (2010) 57–76.
[13] Y. Lee, R. Kopelman, Nanoparticle PEBBLE sensors in live cells, Methods Enzymol. 504 (2012) 419–470.
[14] R. Pan, M. Xu, D. Jiang, J. Burgess, H. Chen, Nanokit for single-cell electrochemical analyses, PNAS 113 (41) (2016) 11436–11440.
[15] A. Tyler, L. Mataseje, C. Urfano, L. Schmidt, K. Antonation, M. Mulvery, C. Corbett, Sequencing device for microbial whole genome sequencing applications, Sci. Rep. 8 (2018) 10931.
[16] M. Amiri, A. Bazaatpour, H. Jafari, R. Boukherroub, S. Szunerits, Electrochemical methodologies for the detection of pathogens, ACS Sens 3 (2018) 1069–1086.
[17] Z. Altintas, M. Gittens, A. Guerreiro, K. Thompson, J. Walker, S. Piletsky, I. Tothill, Detection of waterborne viruses using high affinity molecularly imprinted ploymers, Anal. Chem. 87 (13) (2015) 6801–6807.
[18] Y. Mehmood, What is Limulus Amebocyte Lysate and its ability in endotoxin quantification of pharma products, in: M. Mishra (Ed.), Growing and Handling of Bacterial Cultures, IntechOpen: 2019.
[19] T. Novitsky, Limitations of the Limulus amebocyte lysate test in demonstrating curculating lipopolysaccarides, Ann. N. Y. Acad. Sci. 851 (1998) 416–421.
[20] A. Lakhin, V. Tarantul, L. Gening, Aptamers: problems, solutions and prospects, Acta Naturae 5 (4) (2013) 34–43.
[21] K. Han, Z. Liang, N. Zhou, Design strategies for aptamer-based biosensors, Sensors (Basel) 10 (2010) 4541–4557.
[22] C. Ocaña, M. Pacios, M. del Valle, A reusable impedimetric aptasensor for detection of thrombin employing a graphite-epoxy composite electrode, Sensors (Basel) 12 (2012) 3037–3048.
[23] M.A. Siddiqui, G.M. Keating, Pegaptanib: in exudative age-related macular degeneration, Drugs 65 (11) (2005), pp. 1571–7; discussion 1578–9.
[24] M. Janczuk-Richter, I. Marinovic, J. Niedziolka-Jonsson, K. Szot-Karpinska, Recent applications of bacteriophage-based electrodes: a mini-review, Electrochem. Comm. 99 (2019) 11–15.
[25] A. Rydosz, E. Brzozowska, S. Gorska, K. Wincza, A. Gamian, S. Gruszczynski, A broadband capacitive sensing method for label-free bacterial LPS detection, Biosens. Bioelectron. 75 (2016) 328–336.
[26] J.M. Hicks, R. Halkerston, S.K. Jackson, J.W. Aylott, F.J. Rawson, Real-time bacterial detection with an intracellular ROS sensing platform, Biosens. Bioelctron. 141 (2019) 111430.
[27] F.J. Rawson, J. Hicks, N. Dodd, W. Abate, D.J. Garrett, N. Yip, G. Fejer, A.J. Downard, K.H. Baronian, S.K. Jackson, P.M. Mendes, Fast, ultrasensitive detection of reactive oxygen species using a carbon nanotube based-electrocatalytic intracellular sensor, ACS App. Mat. Int. 7 (42) (2015) 23527–23537.
[28] J.M. Hicks, Z.Y. Wong, D.J. Scurr, N. Silman, S.K. Jackson, P.M. Mendes, J.W. Aylott, F.J. Rawson, Tailoring the electrochemical properties of carbon nanotube modified indium tin oxide via in situ grafting of aryl diazonium, Langmuir 33 (20) (2017) 4924–4933.
[29] F. Rawson, D. Garrett, A. Downard, K. Baronian, Electron transfer from Proteus vulgaris to a covalently assembled, single walled carbon nanotube electrode functionalised with osmium bipyridine complex: application to a whole cell biosensor, Biosens. Bioelctron. 26 (5) (2011) 2383–2389.
[30] F. Rawson, C. Yeung, S. Jackson, P. Mendes, Tailoring 3D single-walled carbon nanotuves anchored to indium tin oxide for natural cellular uptake and intracellular sensing, Nano Lett. 13 (1) (2013) 1–8.
[31] F. Meng, J. Yang, T. Liu, X. Zhu, G. Li, Electric communication between the inner part of a cell and an electrode: the way to look inside a cell, Anal. Chem. 81 (21) (2009) 9168–9171.
[32] A.J. Bard, L. Faulkner, Electrochemical Methods: Fundamentals and Applications, second ed., John Wiley, New York, 2001.
[33] M. Huber, C. Kalis, S. Keck, Z. Jiang, P. Georgel, X. Du, L. Shamel, S. Sovath, S. Mudd, B. Beutler, C. Galanos, M. Freudenberg, R-form LPS, the master key to the activation of TLR4/MD-2 positive cells, Eur. J. Immunol. 36 (3) (2006) 701–711.
[34] A. Płóciennikowska, K. Borzęcka, K. Kwiatkowska, Co-operation of TLR4 and raft proteins in LPS-induced pro-inflammatory signalling, Cell. Mol. Life Sci. 72 (2015) 557–581.
[35] F. Cochet, F. Peri, The role of carbohydrates in the lipopolysaccharide (LPS)/toll-like receptor 4 (TLR4) signalling, Int. J. Mol. Sci. 18 (11) (2017).
[36] B. Zhao, F. Summers, R. Mason, Photooxidation of amplex red to resorufin: implications of exposing the amplex red assay to light, Free Radic. Biol. Med. 53 (5) (2012) 1080–1087.
[37] A. Gomes, E. Fernandes, J.L. Lima, Fluorescence probes used for detection of reactive oxygen species, J. Biochem. Bioph. Methods 65 (2–3) (2005) 45–80.
[38] D. Jacewicz, K. Siedlecka-Kroplewska, J. Drzezdzon, A. Piotrowska, D. Wyrzykowski, A. Tesmar, K. Zamojc, L. Chmurzynski, Method for detection of hydrogen peroxide in HT22 cells, Sci. Rep. 7 (2017) 45673.
[39] E. Ko, V. Tran, Y. Geng, W. Chung, C. Park, M. Kim, G. Jin, G. Seong, Continuous electrochemical detection of hydrogen peroxide by Au-Ag bimetallic nanoparticles in microfluidic devices, J. Electroanal. Chem. 792 (2017) 72–78.
[40] Y. Wang, J. Noel, J. Velmurugan, W. Nogala, M. Mirkin, C. Lu, M. Guille Collignon, F. Lemaitre, C. Amatore, Nanoelectrodes for determination of reactive oxygen and nitrogen species inside murine macrophages, PNAS 109 (29) (2012) 11534–11539.
[41] H. Tavakkoli, M. Akhond, G. Abbas Ghorbankhani, G. Absalan, Electrochemical sensing of hydrogen peroxide using a glassy carbon electrode modified with multiwalled carbon nanotubes and zein nanoparticle composites: application to HepG2 cancer cell detection, Microchim. Acta 187 (105) (2020).